

Mid-infrared photonic crystal cavities in silicon

Raji Shankar,^{1,*} Rick Leijssen,^{1,2} Irfan Bulu,¹ and Marko Lončar¹

¹*School of Engineering and Applied Sciences, Harvard University, Cambridge, Massachusetts 02138, USA*

²*Huygens Laboratory, Leiden University, P.O. Box 9504, 2300 RA Leiden, Netherlands*

*shankar2@fas.harvard.edu

Abstract: We demonstrate the design, fabrication, and characterization of silicon photonic crystal cavities realized in a silicon on insulator (SOI) platform, operating at a wavelength of 4.4 μm with a quality factor of 13,600. Cavity modes are imaged using the technique of scanning resonant scattering microscopy. To the best of our knowledge, this is the first demonstration of photonic devices fabricated in SOI and operating in the 4–5 μm wavelength range.

©2011 Optical Society of America

OCIS codes: (230.5750) Resonators; (230.5298) Photonic crystals; (350.4238) Nanophotonics and photonic crystals.

References and links

1. C. Tsay, E. Mujagić, C. K. Madsen, C. F. Gmachl, and C. B. Arnold, "Mid-infrared characterization of solution-processed As₂S₃ chalcogenide glass waveguides," *Opt. Express* **18**(15), 15523–15530 (2010), <http://www.opticsinfobase.org/abstract.cfm?URI=oe-18-15-15523>.
2. R. Soref, "Mid-infrared photonics in silicon and germanium," *Nat. Photonics* **4**(8), 495–497 (2010).
3. R. A. Soref, S. J. Emelett, and A. R. Buchwald, "Silicon waveguided components for the long-wave infrared region," *J. Opt. A, Pure Appl. Opt.* **8**(10), 840–848 (2006).
4. S. Zlatanovic, J. S. Park, S. Moro, J. M. C. Boggio, I. B. Divliansky, N. Alic, S. Mookherjea, and S. Radic, "Mid-infrared wavelength conversion in silicon waveguides using ultracompact telecom-band-derived pump source," *Nat. Photonics* **4**(8), 561–564 (2010).
5. B. Jalali, "Silicon Photonics Nonlinear Optics in the Mid-Infrared," *Nat. Photonics* **4**(8), 506–508 (2010).
6. V. Raghunathan, D. Borlaug, R. R. Rice, and B. Jalali, "Demonstration of a Mid-infrared silicon Raman amplifier," *Opt. Express* **15**(22), 14355–14362 (2007), <http://www.opticsinfobase.org/oe/abstract.cfm?uri=oe-15-22-14355>.
7. X. P. Liu, R. M. Osgood, Y. A. Vlasov, and W. M. J. Green, "Mid-infrared optical parametric amplifier using silicon nanophotonic waveguides," *Nat. Photonics* **4**(8), 557–560 (2010).
8. T. Baehr-Jones, A. Spott, R. Ilic, A. Spott, B. Penkov, W. Asher, and M. Hochberg, "Silicon-on-sapphire integrated waveguides for the mid-infrared," *Opt. Express* **18**(12), 12127–12135 (2010), <http://www.opticsinfobase.org/abstract.cfm?URI=oe-18-12-12127>.
9. A. Spott, Y. Liu, T. Baehr-Jones, R. Ilic, and M. Hochberg, "Silicon waveguides and ring resonators at 5.5 μm ," *Appl. Phys. Lett.* **97**(21), 213501 (2010).
10. Y. Akahane, T. Asano, B. S. Song, and S. Noda, "High-Q photonic nanocavity in a two-dimensional photonic crystal," *Nature* **425**(6961), 944–947 (2003).
11. P. B. Deotare, M. W. McCutcheon, I. W. Frank, M. Khan, and M. Loncar, "High quality factor photonic crystal nanobeam cavities," *Appl. Phys. Lett.* **94**(12), 121106 (2009).
12. M. W. McCutcheon, G. W. Rieger, I. W. Cheung, J. F. Young, D. Dalacu, S. Frederick, P. J. Poole, G. C. Aers, and R. L. Williams, "Resonant scattering and second-harmonic spectroscopy of planar photonic crystal microcavities," *Appl. Phys. Lett.* **87**(22), 221110 (2005).
13. M. Galli, S. L. Portalupi, M. Belotti, L. C. Andreani, L. O'Faolain, and T. F. Krauss, "Light scattering and Fano resonances in high-Q photonic crystal nanocavities," *Appl. Phys. Lett.* **94**(7), 071101 (2009).
14. M. Notomi, A. Shinya, S. Mitsugi, G. Kira, E. Kuramochi, and T. Tanabe, "Optical bistable switching action of Si high-Q photonic-crystal nanocavities," *Opt. Express* **13**(7), 2678–2687 (2005).
15. T. M. Babinec, B. J. M. Hausmann, M. Khan, Y. A. Zhang, J. R. Maze, P. R. Hemmer, and M. Loncar, "A diamond nanowire single-photon source," *Nat. Nanotechnol.* **5**(3), 195–199 (2010).

1. Introduction

The mid-infrared (IR) wavelength range (2–20 μm) has recently become more accessible due to the development of high-power, room-temperature operational sources and sensitive detectors. At the same time, little work has been done in developing passive photonic

elements such as waveguides, resonators, splitters, etc. for the mid-IR. However, integrated photonics at this wavelength range would be useful for a variety of applications for which the mid-IR is particularly suited, including thermal imaging, biological sensing, chemical bond spectroscopy, free space communications and trace gas sensing.

Conventionally, mid-IR photonics is associated with the III-IV materials used for active optoelectronic devices (lasers and detectors), as well as chalcogenide glasses used for passive photonic elements [1]. However, it has recently been proposed by R. Soref that silicon is also a promising material for the mid-IR, as it exhibits low loss throughout much of the mid-IR [2,3]. Using silicon as the material of choice for the mid-IR would allow us to take advantage of well-developed fabrication techniques and CMOS compatibility, making the realization of on-chip integrated mid-IR devices more realistic. Finally, due to the lack of two- and three-photon absorption in the mid-IR, the power density of optical signals propagating in Si waveguides or stored in Si optical cavities can be significantly higher than at the near-IR wavelengths used for telecommunications [4–7]. Therefore, Si-based on-chip optical networks operating in mid-IR may find applications as optical interconnects for datacom. Silicon-on-sapphire waveguides [8] and ring resonators [9] have already been demonstrated in the past year. In this work, we demonstrate the first wavelength-scale optical resonators, in the form of L3 photonic crystal cavities [10], in the CMOS compatible silicon-on-insulator material platform. High quality factor (Q) and low mode volume optical resonators in the mid-IR are of interest for many applications including trace gas sensing, optical interconnects, and so on.

2. Design

We chose the well-known L3 cavity design [10] for our photonic crystal cavities due to the relative ease of free-space in- and out-coupling in this cavity (Fig. 1). This cavity design consists of a two-dimensional hexagonal photonic crystal lattice of air holes in a Si slab, with three central air holes removed to form a line defect. Bragg scattering accounts for electromagnetic confinement in the x and y directions, while index contrast provides confinement in the z direction. The cavity mode is linearly polarized. To further achieve confinement of the light to the cavity region, the air holes on either side of the cavity are shifted outwards, decreasing the phase mismatch between the cavity region and the Bragg mirror region formed by the photonic crystal (Fig. 1a). This allows for higher quality (Q) factors to be achieved [10].

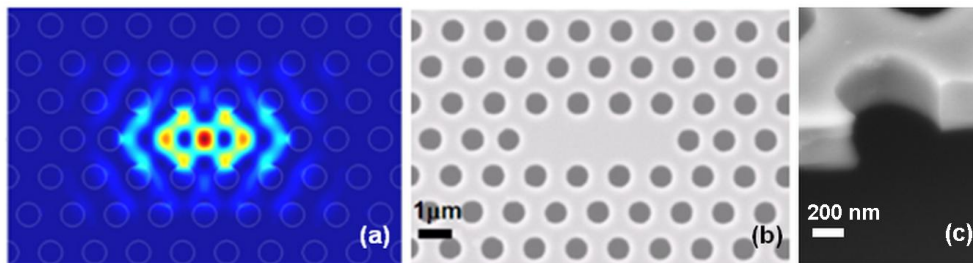


Fig. 1. (a) Mode profile of E_z field component of L3 photonic crystal cavity with $a = 1.34 \mu\text{m}$, $r = 0.263a$, $t = 0.5 \mu\text{m}$, and hole shift $s = 0.15a$, with resonance wavelength of $4.604 \mu\text{m}$ and Q factor of 24,000. (b) Scanning electron micrograph of fabricated L3 photonic crystal cavity. (c) Scanning electron micrograph of etched sidewall of photonic crystal cavity hole; image is taken at 45° tilt.

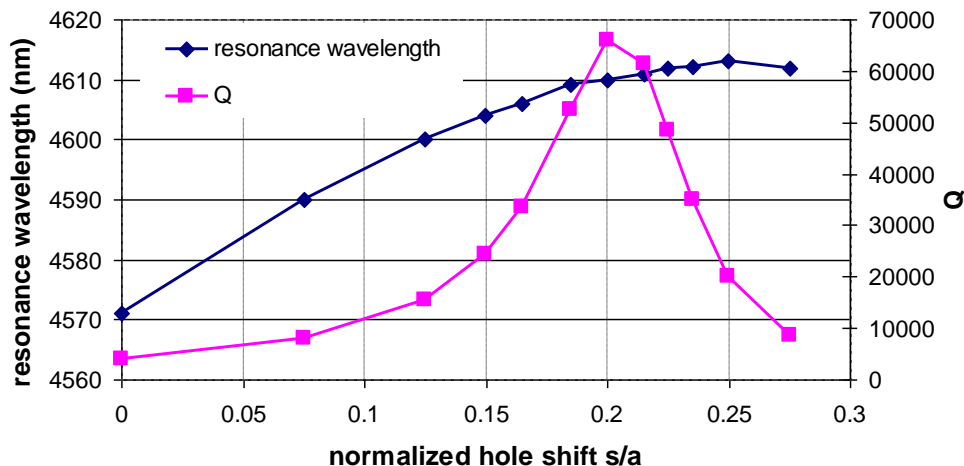


Fig. 2. Results of FDTD calculations showing L3 photonic crystal cavity resonance wavelengths and quality factors as a function of s , the hole shift.

The cavities were designed using three-dimensional finite-difference time-domain method (Lumerical Solutions, Inc.) for a Si device layer thickness t of 500 nm. The periodicity of the photonic crystal lattice is $a = 1.34 \mu\text{m}$, and the air hole radius $r = 353 \text{ nm}$ ($r/a = 0.263$). The air hole shift s was scanned from zero shift to a maximum shift of $0.275a$ in order to optimize the Q factor of the cavity. An air hole shift of $s = 0.2a$ results in an optimal design at $\lambda = 4.615 \mu\text{m}$ with a Q factor of 66,000 when 10 mirror hole pairs surround the cavity region. The mode profile is plotted in Fig. 1a, and the theoretical calculations for the resonance wavelength and Q factor as a function of s are shown in Fig. 2. As expected, as the hole shift is increased, the cavity resonance is pushed to longer wavelengths, due to the increase in high-dielectric material in the cavity region.

3. Fabrication

The devices were fabricated on a silicon-on-insulator (SOI) substrate (SOITEC Inc.), with a device layer thickness of 500 nm and SiO_2 layer thickness of $3 \mu\text{m}$. ZEP (Zeon Corp), a positive electron-beam resist, was used as a mask for electron-beam lithography. The film was deposited by spinning pure ZEP onto the substrate at a rate of 2000 rpm, followed by a post-spin bake at 180°C for 3 minutes, resulting in a film thickness of 550 nm. A standard 100 kV electron beam lithography tool (Elionix ELS-7000) was used to define patterns in the ZEP layer, which were then developed in o-xylene for 40 seconds followed by a rinse in isopropanol alcohol. Etching was performed in a reactive ion etcher (STS-ICP-RIE) using C_4F_8 , SF_6 , and H_2 gases in a two step process. The first step was a Si etch step at 10 mTorr with a C_4F_8 flow rate of 130 sccm, a SF_6 flow rate of 80 sccm, and no H_2 flow. The second step was a Si and SiO_2 etch step at 20 mTorr with a C_4F_8 flow rate of 130 sccm, SF_6 flow rate of 80 sccm, and a H_2 flow rate of 15 sccm. The devices were undercut using a 7:1 buffered oxide etch for 45 minutes. A scanning electron micrograph of a completed device is shown in Fig. 1b. A number of different L3 photonic crystal cavities were fabricated by varying the air hole shift, resulting in cavities with different quality factors and resonance wavelengths as described earlier. Sets of cavity with both four mirror hole pairs and ten mirror hole pairs were fabricated.

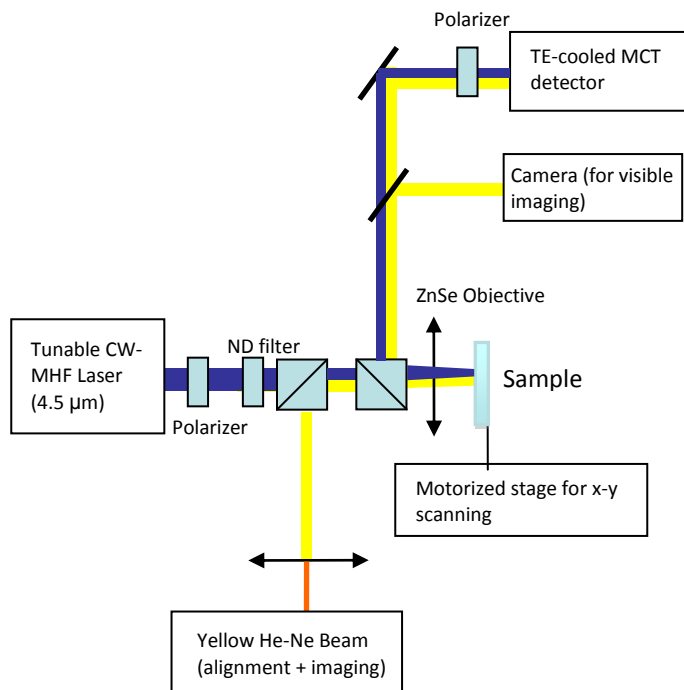


Fig. 3. Schematic of experimental setup used for resonant scattering-based characterization of photonic crystal cavities.

4. Characterization

We used the resonant scattering method [11,12] to test our cavities (Fig. 3). Light from a tunable quantum cascade laser (QCL) with emission from 4.315 to 4.615 μm (Daylight Solutions, Inc.) is sent into a ZnSe objective lens with numerical aperture (NA) of 0.22 and focused onto the sample, which is placed so that the cavity mode polarization is oriented at 45 degrees with respect to the E-field of the laser spot. Since the QCL emission is invisible, a yellow HeNe laser beam was aligned to the path of the QCL and then used to align the rest of the optics. A Ge neutral density filter with optical density of 1.0 is used to reduce the light intensity. The sample is mounted on an automatic micropositioner stage, which can be scanned using computer control. The light that is coupled and re-emitted by the photonic crystal cavities is backscattered into the ZnSe objective, and then travels through a second polarizer (the analyzer) which is cross-polarized with respect to the input polarizer, before being focused onto a thermoelectrically cooled mercury cadmium telluride (MCT) detector. This cross-polarization method enhances the signal-to-background ratio of the resonantly scattered light (the signal) to the non-resonantly scattered light (the background). Depending on this ratio, the resonance peak can appear as a Lorentzian or a Fano lineshape caused by the phase shift between the resonant (re-emitted by cavity) and non-resonant components of the back-scattered signal [13].

The experimental results for photonic crystal cavities with 10 mirror hole pairs are shown in Fig. 4. Photonic crystal cavity modes are found within the range of 4.38 to 4.42 μm . As predicted by theory (Fig. 2), the cavity resonance wavelengths redshift as the air hole shift s is increased from zero to a maximum of $s = 0.225a$ (Fig. 4b). The Q-factors also roughly follow the trend predicted by theory. A peak Q-factor of 13,600 is found for $s = 0.15a$, representing

the highest Q factor measured for any Si-based optical cavity in the mid-infrared (Fig. 4b). The inset in Fig. 4a shows the measured Fano lineshape of the resonance along with the theoretical fit $F(f)$ [13] given by:

$$F(f) = A_0 + F_0 \frac{[q + 2(f - f_0)/\Gamma]^2}{1 + [2(f - f_0)/\Gamma]^2}, \quad (1)$$

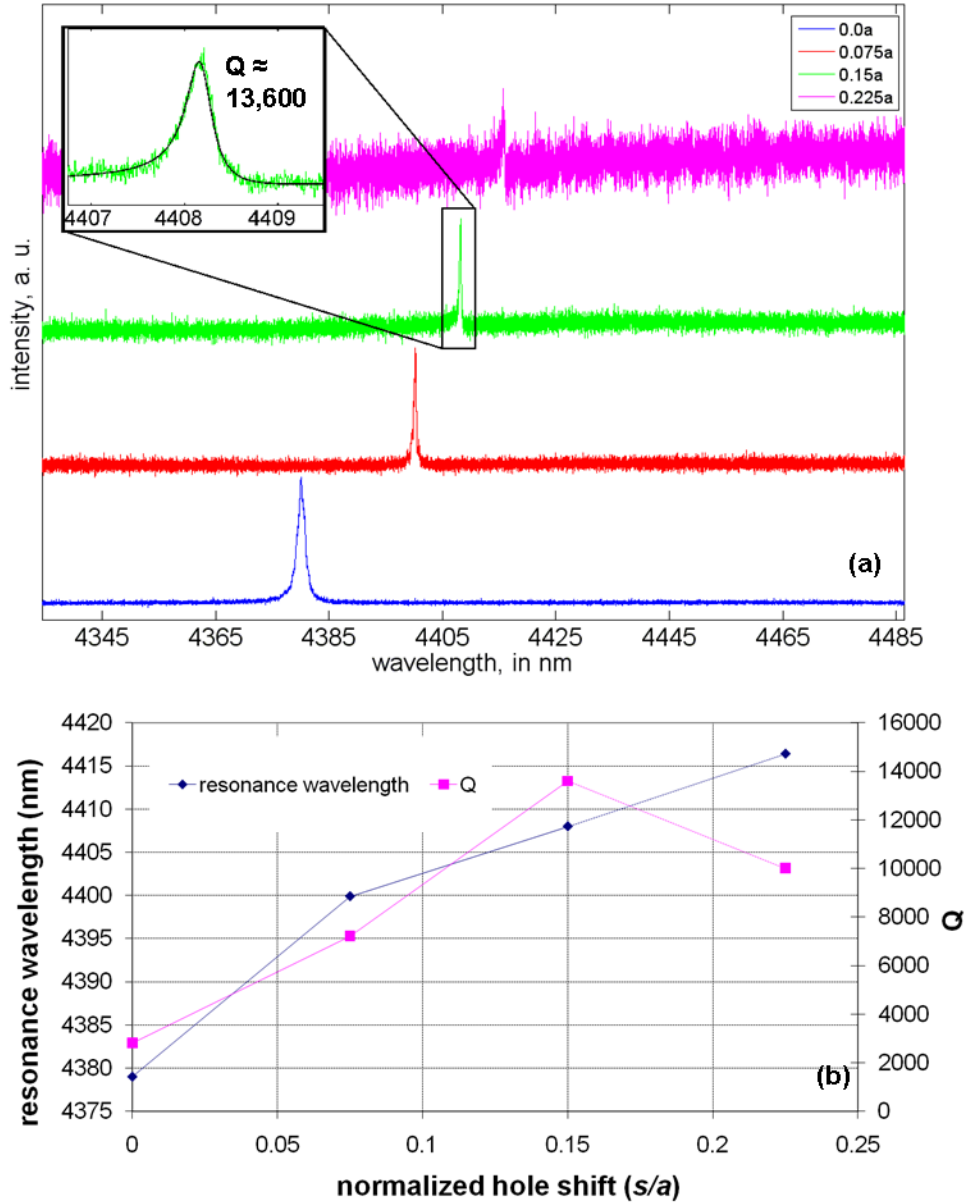


Fig. 4. (a) Resonant scattering spectra of photonic crystal cavities with $s = 0$, $s = 0.075a$, $s = 0.15a$, $s = 0.225a$. Scale is linear. Inset shows Fano fit to $s = 0.15a$ cavity. Fitting parameters are $A_0 = 5.6e-5$, $q = 2.52$, $\Gamma = 5.0$ GHz, $f_0 = 68$ THz, and $F_0 = 0.0013$. Cavity with $s = 0.2a$ did not show a resonance. (b) resonance wavelength and Q vs. s for measured cavities. A peak Q of 13,600 is measured at 4408 nm. Lines between points are there to guide the eye.

where A_0 and F_0 are constants, q is the Fano parameter, f_0 is the cavity mode frequency, and Γ is the linewidth. The fit is plotted in terms of the wavelength $\lambda = c/f$, where c is the velocity of light. We extract the quality factor from the ratio of f_0 to Γ . In the case of the $s = 0.15a$ cavity, the extracted linewidth was 5.0 GHz with a f_0 of 68 THz. In the $s = 0.2a$ cavity we did not detect a resonance, possibly due to the low NA (0.22) of the ZnSe objective used to collect light. With a low NA lens, it is difficult to couple light into and collect light from higher-Q cavities, where the cavity emission is largely at angles outside the collection cone of the lens [11]. This is also the reason why the resonance for $s = 0.225a$ (magenta in Fig. 4a) has a poor signal-to-noise ratio. Part of the challenge of working in the mid-IR is the paucity of high-quality optical components, such as high numerical aperture objective lenses, more readily available at other wavelength regimes. This also results in a large focal spot size, approximately 20 μm in diameter. In order to improve signal-to-noise ratio in our experiments, we could increase the excitation power of our laser. However, when the QCL output power was increased to 100 mW (only about 3-5% of this power gets coupled into the cavity), we noticed the evidence of optical bistability in our photonic crystal cavities [14]. We believe the origin of this nonlinear effect is thermo-optic in nature, and is most likely due to the finite linear absorption of Si in the mid-infrared [3]. We are exploring this bistability for future work.

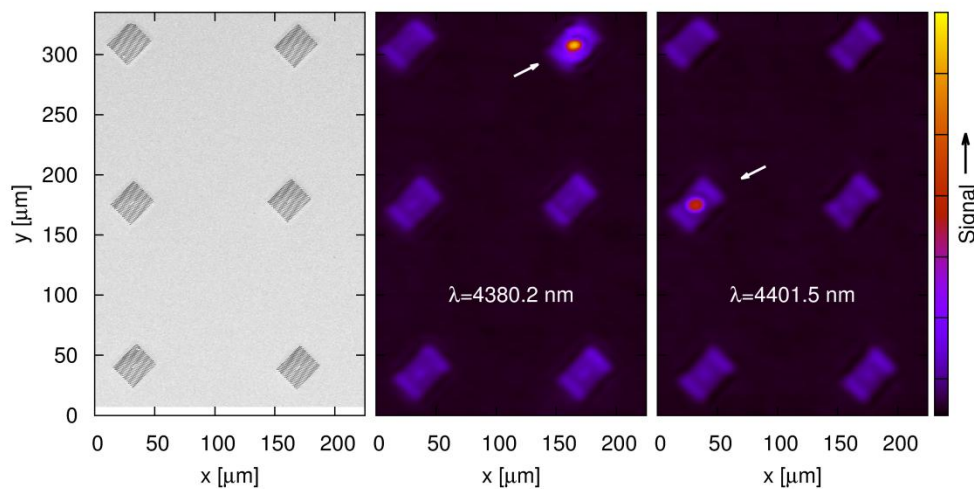


Fig. 5. Mid-infrared scanning resonant scattering image of an array of 5 cavities (upper left hand structure is photonic crystal with no cavity). Scanning electron micrograph is provided for comparison. When our laser is tuned to one of the cavity resonances, and scanned over the cavity array, only the cavity in resonance with the laser lights up. For example, when 4380.2 nm light, corresponding to the resonance of the top right cavity in the center panel, is scanned over the array, only that cavity appears “ON”, featuring a bright spot in its center. Alternatively, when the laser is tuned to 4401.5nm and scanned over the array, only the middle-left cavity (rightmost panel) resonates.

In order to further confirm that the observed resonances are indeed associated with cavity modes, it is important to visualize their spatial profiles. However, since no true viewer cards exist for the mid-IR wavelength range, and mid-IR cameras are rather expensive, we adapted the scanning-confocal microscopy approach to image our devices [15]. We call this method scanning resonant scattering microscopy. A single mid-IR detector is used, and the spatial profile is obtained by scanning the sample in x- and y-direction using computer-controlled micropositioners. In order to locate the cavities, we scan the sample stage in both x- and y-directions at an arbitrary wavelength. The outlines of the cavities can be made out at all wavelengths, so we can then move to the center of the photonic crystal cavity region and

sweep the laser in wavelength in order to obtain a resonant scattering spectrum. This procedure allows us to precisely position the laser beam onto our cavities. Furthermore, we can obtain the image of the cavity resonance by tuning the laser to the cavity resonance and moving the sample holder stages in the x- and y-directions and recording the detector reading at each position. Images obtained using this approach are shown in Fig. 5. It can be seen that the cavity regions light up at the wavelengths corresponding to the resonance peak in the wavelength scan, and remain dark off-resonance, confirming that the peaks we see in the wavelength scans do indeed correspond to L3 photonic crystal cavity modes. In effect, this imaging approach can be seen as a single-pixel mid-infrared camera, allowing for the visualization of fabricated structures and resonant modes without the use of extremely expensive mid-IR cameras that are commercially available.

In Fig. 6, we show a spectrum and scanning mid-IR images of additional resonances that were observed in our four-mirror hole pair devices. These devices were placed relatively close together, with a separation of 22 μm in the y-direction. Resonant scattering spectra of these cavity devices show two extra peaks appearing (at 4.433 μm and 4.567 μm) in addition to the cavity resonance peak (4.444 μm). Using our scanning resonant scattering microscopy technique, we were able to image these modes and attribute them to the inter-cavity resonances of the Fabry-Perot cavity formed between two adjacent photonic crystal structures (Fig. 6b): one resonance has an anti-node (leftmost panel, 4.433 μm) and the other one has a node (rightmost panel, 4.567 μm) in the center of the inter-cavity region. The resonance at 4.444 μm (center panel in Fig. 6b) corresponds to a bonafide resonance of the L3 photonic crystal cavity.

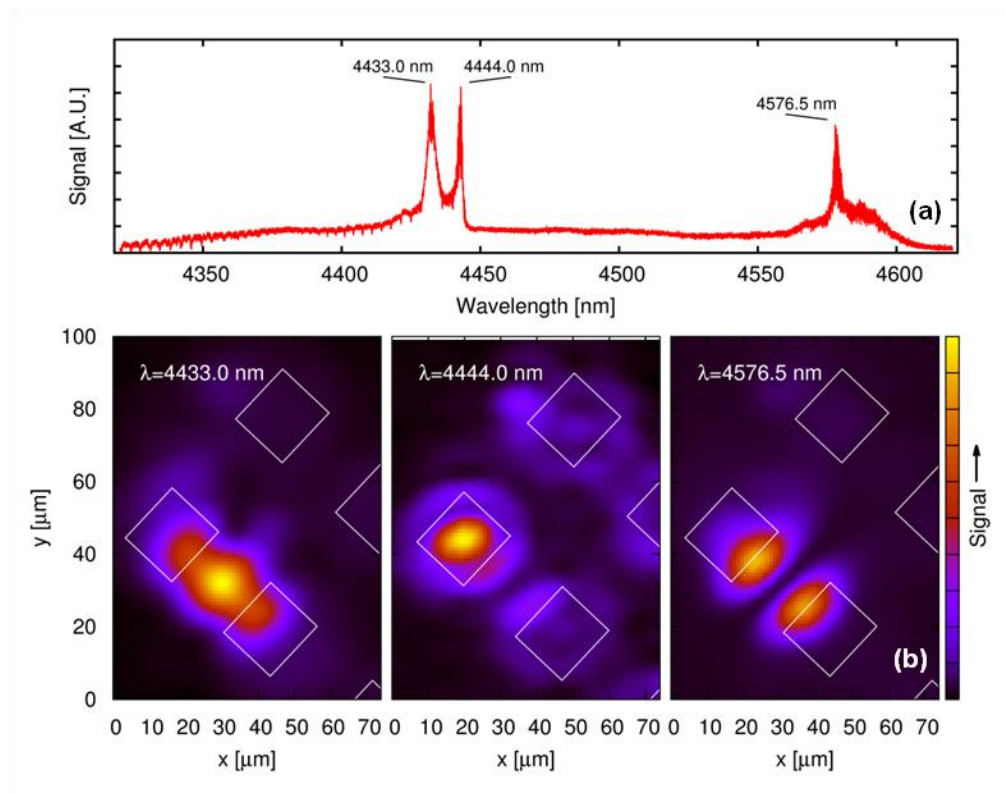


Fig. 6. (a) Resonant scattering spectrum showing peaks corresponding to two inter-cavity Fabry-Perot resonances (4430.0 nm and 4567.5 nm) and one L3 photonic crystal cavity resonance (4444.0 nm). (b) scanning images of Fabry-Perot resonances (leftmost and right most panels) and photonic crystal cavity resonance (center panel).

The ability to accurately image the spatial profile of resonances observed in the collected spectra, and therefore unambiguously attribute them to the modes of different cavities, is an important demonstration of the utility of the mid-IR scanning resonant scattering microscopy that we developed. The combination of scanning microscopy and resonant scattering wavelength measurements results in a very powerful tool that overcomes many of the difficulties inherent in working at the mid-IR. Iterating between scanning microscopy and wavelength scanning allows us to optimize our resonant scattering spectra signals more quickly and accurately than we would be able to with only a CCD camera sensitive to visible wavelengths to guide us as to the location of our cavities. We see scanning resonant scattering microscopy as an essential tool in a mid-IR toolbox.

5. Conclusion

In conclusion, we have demonstrated the design, fabrication, and characterization of silicon-based photonic crystal cavities for the mid-infrared, with a peak quality factor of 13,600. In addition, we have transferred experimental techniques used at telecommunication and visible wavelengths, most notably resonant scattering and scanning confocal microscopy, to characterize our mid-IR cavities. Further work will be focused on achieving higher quality factor cavities and in coupling mid-IR photonic crystal cavities to waveguides so that the vision of on-chip integrated photonics in the mid-infrared can be attained. Such a fully integrated platform would enable realization of chip-scale systems for trace gas sensing, optical-wireless, on-chip optical interconnects, phased-arrays for LIDAR applications, and so on.

Acknowledgments

The authors would like to thank Leonard Kogos for his help with the experimental setup, and Qimin Quan for many helpful discussions. This work is supported in part by the NSF CAREER grant (ECCS-0846684) and generous support from Schlumberger-Doll Research Center (Cambridge, MA). Device fabrication was performed at the Center for Nanoscale Systems at Harvard University. R. S. would like to thank the NSF GRFP.